

WASP-190b: Tomographic discovery of a transiting hot Jupiter

L. Y. TEMPLE,¹ C. HELLIER,¹ D.R. ANDERSON,¹ F. BOUCHY,² D.J.A. BROWN,^{3,4} A. BURDANOV,⁵
A. COLLIER CAMERON,⁶ L. DELREZ,⁷ M. GILLON,⁵ E. JEHIN,⁵ M. LENDL,^{8,2} P.F.L. MAXTED,¹ L. D. NIELSEN,²
F. PEPE,² D. POLLACCO,^{3,4} D. QUELOZ,⁹ D. SÉGRANSAN,² B. SMALLEY,¹ A.H.M.J. TRIAUD,¹⁰ O.D. TURNER,^{2,1}
S. UDRY,² AND R.G. WEST³

¹*Astrophysics Group, Keele University, Staffordshire, ST5 5BG, UK*

²*Observatoire astronomique de l'Université de Genève
51 ch. des Maillettes, 1290 Sauverny, Switzerland*

³*Department of Physics, University of Warwick,
Gibbet Hill Road, Coventry, CV4 7AL, UK*

⁴*Centre for Exoplanets and Habitability, University of Warwick,
Gibbet Hill Road, Coventry CV4 7AL, UK*

⁵*Space sciences, Technologies and Astrophysics Research (STAR) Institute,
Université de Liège, Allée du 6 Août 17, 4000 Liège, Belgium*

⁶*SUPA, School of Physics and Astronomy, University of St. Andrews
North Haugh, Fife, KY16 9SS, UK*

⁷*Cavendish Laboratory, J J Thomson Avenue,
Cambridge, CB3 0HE, UK*

⁸*Space Research Institute, Austrian Academy of Sciences, Schmiedlstr. 6, 80 42, Graz, Austria*

⁹*Cavendish Laboratory, J J Thomson Avenue, Cambridge, CB3 0HE, UK*

¹⁰*School of Physics & Astronomy, University of Birmingham, Edgbaston, Birmingham, B15 2TT, UK*

Submitted to AJ

ABSTRACT

We report the discovery of WASP-190b, an exoplanet on a 5.37-day orbit around an inflated F6 IV-V star with $T_{\text{eff}} = 6400 \pm 100$ K, $M_{\star} = 1.35 \pm 0.05 M_{\odot}$ and $R_{\star} = 1.6 \pm 0.1 R_{\odot}$. The planet has a radius of $R_{\text{p}} = 1.15 \pm 0.09 R_{\text{Jup}}$ and a mass of $M_{\text{p}} = 1.0 \pm 0.1 M_{\text{Jup}}$, making it a mildly inflated hot Jupiter. The orbit is also marginally misaligned with respect to the stellar rotation, with $\lambda = 21 \pm 6^{\circ}$ measured using Doppler tomography. We compare a Rossiter-McLaughlin analysis (involving radial velocity measurements) with the Doppler tomography method, and find that the latter provides a better constraint on $v \sin i_{\star}$ and λ .

Keywords: planets and satellites: detection — planets and satellites: individual (WASP-190b) — stars: individual (WASP-190)

1. INTRODUCTION

The Rossiter-McLaughlin (RM) effect, a distortion of the line profiles of a star caused by an occulting body blocking part of the stellar face, was first detected for a transiting hot Jupiter by Queloz et al. (2000) in observations of HD 209458. It has since been used extensively to measure the projected angle between the planet's orbit

and the stellar rotation axis in many hot-Jupiter systems (e.g. Triaud 2017).

One can also plot the line profiles as a function of phase, looking for the Doppler shadow of the planet as it moves across the line profiles. This “tomographic” method was first used in the discovery of a planet for WASP-33b (Collier Cameron et al. 2010b). The tomographic technique is particularly useful for systems with hotter and fast-rotating stars, with fewer and broader spectral lines, which may give only less-accurate radial-velocity measurements. Thus it has now been used in the discovery of hot Jupiters transiting hot stars, including

KELT-20b (Lund et al. 2017), HAT-P-67b (Zhou et al. 2017), WASP-167b/KELT-13b (Temple et al. 2017), MASCARA-1b (Talens et al. 2017) and WASP-189b (Anderson et al. 2018).

Brown et al. (2017) compare tomographic and RM analyses of the same datasets for six WASP systems. They find that the tomographic method consistently gives better constraints on values for the projected stellar rotational velocity $v \sin i_\star$ and the sky-projected obliquity angle λ . Note that the tomographic analysis method uses the line profiles more directly, while an RM analysis in terms of radial-velocity measurements (RVs) needs one to translate the change in the line profiles owing to a planet shadow into a change in the overall radial velocity (Hirano et al. 2011; Boué et al. 2013).

In this work, we report the discovery and characterisation of WASP-190b, a hot Jupiter orbiting a star of $T_{\text{eff}} = 6400$ K which can be found in *TESS* Sector 2 as TIC ID:116156517 (Ricker et al. 2015; Stassun et al. 2018). We use both tomographic and RM analyses to determine the geometry of the system, and confirm the existence of the planet via the detection of its Doppler shadow and by measuring its mass using orbital RV measurements.

2. DATA AND OBSERVATIONS

We observed WASP-190 using the WASP-South telescope (Hellier et al. 2011) at the South African Astronomical Observatory (SAAO) from 2006 to 2011. After the detection of a planet-like transit dip in the WASP lightcurve we confirmed the transit with a follow-up lightcurve obtained using the TRAPPIST-South telescope (Jehin et al. 2011), and proceeded to obtain reconnaissance spectroscopy with the Euler/CORALIE spectrograph (Queloz et al. 2001). These were sufficient to rule out a stellar-mass binary, but with relatively large errors were consistent with no motion and were inconclusive about whether the transiting body was a planet.

We thus attempted tomography of a transit, obtaining a series of 28 spectra through transit on the night of 2017 October 13 using the ESO 3.6-m/HARPS spectrograph (Pepe et al. 2002), accompanied by simultaneous photometry using the SPECULOOS-Europa telescope (Burdanov et al. 2018; Gillon 2018; Delrez et al. 2018). After tomographic detection of a planet-like signal, we obtained 5 further orbital RVs with HARPS to constrain the planetary mass.

The HARPS spectra were cross-correlated over a window of ± 350 km s⁻¹, using a mask matching a G2 spectral type, and the standard HARPS Data Reduction Software as described by Baranne et al. (1996), Pepe et al. (2002). We then analysed the cross-correlation

Table 1. Observations of WASP-190b.

Telescope/Instrument	Date	Notes
WASP-South	2006–2011	30137 pts.
TRAPPIST-South	2014 Nov 26	<i>I+z</i> , 7s exp.
SPECULOOS-Europa	2017 Oct 13	<i>I+z</i> , 10s exp.
CORALIE	2014 Aug–Oct	5 RVs
HARPS	2017 Oct 13	28 spectra taken including a transit
HARPS	2018 Oct	5 RVs

functions (CCFs) themselves, and computed radial velocity (RV) measurements from the CCFs.

We used the WASP photometric data to look for any evidence of rotational modulation of the host star, using the methods of Maxted et al. (2011). We find no such variability at periods longer than a day, with a 95%-confidence upper limit on the amplitude of 1 mmag.

3. STELLAR PARAMETERS FROM SPECTRAL ANALYSIS

In order to determine stellar parameters of WASP-190 we co-added the HARPS spectra obtained on the night of 2017 October 13 and performed a spectral analysis. We adopted a microturbulent velocity of $v_{\text{mic}} = 1.6$ km s⁻¹ from the calibration of Bruntt et al. (2010) and a macroturbulent velocity of $v_{\text{mac}} = 6.5$ km s⁻¹ from the calibration of Doyle et al. (2014). We used the H α line to determine an effective temperature $T_{\text{eff}} = 6400 \pm 100$ K, while using the Na D feature to measure $\log g_* = 3.9 \pm 0.1$. We also determined the projected stellar rotational velocity $v \sin i_\star = 13.8 \pm 0.7$ km s⁻¹, and the surface metallicity $[\text{Fe}/\text{H}] = -0.02 \pm 0.05$. These results are also listed in Table 3. Using the MKCLASS program (Gray & Corbally 2014) we then obtained a spectral type of F6 IV–V.

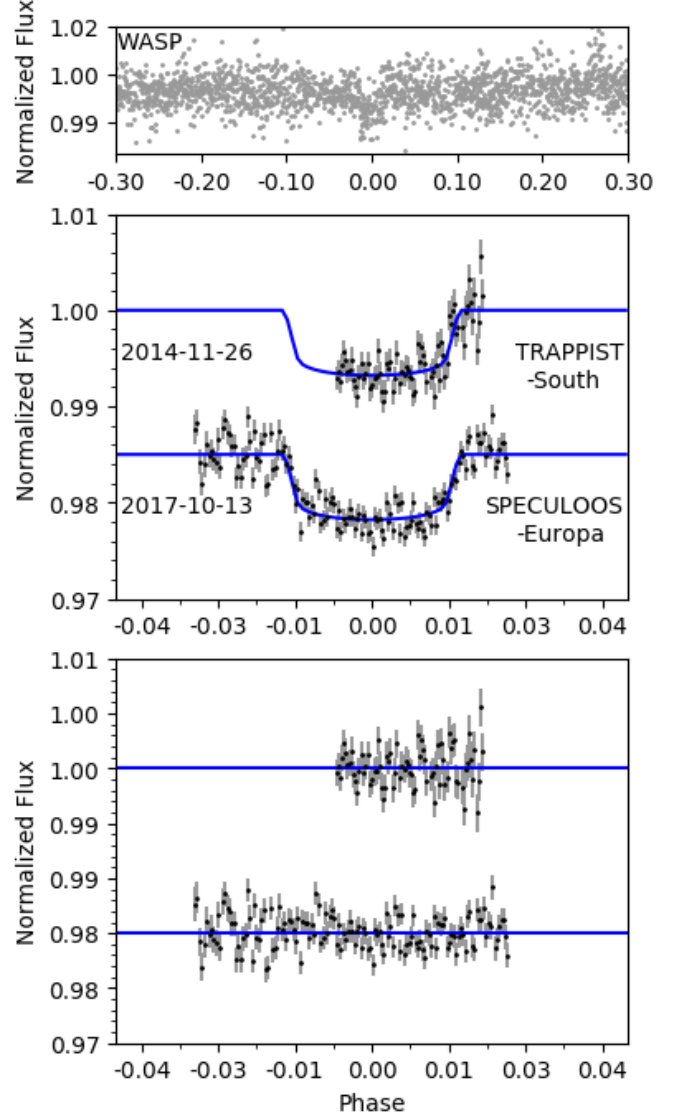
4. COMBINED MCMC ANALYSIS

We conduct an analysis very similar to that conducted by Temple et al. (2018) for WASP-174b, which involves the use of Markov Chain Monte Carlo (MCMC) methods to analyse the combined photometric and spectroscopic datasets. As one approach we use the in-transit spectroscopy data in the form of RV measurements, following the method of Hirano et al. (2011), and as a second approach we use the same data in the form of CCFs, following methods similar to that used by Brown et al. (2017); Temple et al. (2017). We call the former the Rossiter–McLaughlin (RM) analysis and the latter the tomographic analysis.

The code we use is described by Collier Cameron et al. (2007) and Pollacco et al. (2008), which in the latest ver-

Table 2. RV measurements of WASP-190, taken using the CORALIE and HARPS spectrographs for this work.

BJD_{TDB}	RV	σ_{RV}	BS	σ_{BS}
	(km s^{-1})	(km s^{-1})	(km s^{-1})	(km s^{-1})
CORALIE (out of transit):				
6871.794771	0.89	0.05	-0.07	0.10
6895.811527	0.94	0.05	-0.16	0.10
6922.731329	0.90	0.03	-0.05	0.06
6952.511870	0.95	0.04	0.15	0.08
7000.625106	0.87	0.04	-0.22	0.08
8392.595422	0.84	0.07	-0.24	0.14
HARPS (including a transit):				
8040.529251	0.84	0.02	0.04	0.04
8040.540026	0.82	0.02	-0.04	0.04
8040.550489	0.84	0.02	0.05	0.04
8040.561472	0.86	0.02	-0.02	0.04
8040.572351	0.85	0.02	-0.05	0.04
8040.582918	0.85	0.02	-0.02	0.04
8040.593797	0.87	0.02	-0.00	0.04
8040.604572	0.92	0.02	0.02	0.04
8040.615243	0.89	0.02	-0.07	0.04
8040.626122	0.90	0.02	-0.13	0.04
8040.636897	0.87	0.02	-0.06	0.04
8040.647776	0.84	0.02	-0.01	0.04
8040.658459	0.80	0.02	-0.02	0.04
8040.669130	0.79	0.02	0.04	0.04
8040.680113	0.80	0.02	0.10	0.04
8040.690784	0.80	0.02	0.03	0.04
8040.701350	0.78	0.02	-0.07	0.04
8040.712334	0.76	0.02	-0.03	0.04
8040.723016	0.73	0.02	-0.03	0.04
8040.733791	0.76	0.02	-0.05	0.04
8040.744670	0.73	0.03	-0.05	0.06
8040.755341	0.76	0.03	0.05	0.06
8040.766220	0.77	0.03	0.09	0.06
8040.777100	0.81	0.03	-0.10	0.06
8040.787770	0.83	0.03	-0.02	0.06
8040.798545	0.82	0.03	0.10	0.06
8040.809112	0.85	0.03	-0.06	0.06
8040.820107	0.82	0.03	0.06	0.06
HARPS (out of transit):				
8393.843700	0.92	0.01	-0.20	0.02
8396.706300	0.73	0.01	0.10	0.02
8397.590800	0.86	0.04	-0.15	0.08
8398.611000	0.92	0.02	-0.24	0.04
8399.542350	0.85	0.04	-0.13	0.08

**Figure 1.** Top: the discovery lightcurve for WASP-190b (WASP-South). Middle: the two follow-up lightcurves with the best-fitting model shown in blue. Bottom: the residuals of the fits to the follow-up lightcurves.

sion includes the tomographic analysis as described by Collier Cameron et al. (2010a). In both analyses, fitting the photometric lightcurves allows direct measurement of the planet-to-star area ratio $(R_p/R_\star)^2$, the impact parameter b and the key transit timing information T_C , P , T_{14} and $T_{12}(T_{34})$, which are respectively the epoch of mid-transit, the orbital period, the transit duration and the duration of ingress(egress). We use the value of T_{eff} obtained in the spectral analysis (see discussion in Section 7) as input, and for each new value of T_{eff} we interpolate four-parameter law limb-darkening coefficients from the tables of Claret (2000, 2004). Stellar mass is

Table 3. All system parameters obtained in the combined analyses for WASP-190b .

1SWASP J003050.23–403424.3		
2MASS 00305023–4034243		
TIC ID:116156517		
Gaia DR2 4994237247949280000		
RA = 00 ^h 30 ^m 50.233 ^s , Dec = –40°34′24.36″ (J2000)		
$V = 11.7 \pm 0.1$ (TYCHO2)		
Gaia DR2 Proper Motions:		
(RA) 38.23 ± 0.03 (Dec) -9.14 ± 0.04 mas/yr		
Gaia DR2 Parallax: 1.82 ± 0.03 mas		
Rotational Modulations: < 1 mmag (95%)		
<i>Stellar parameters from spectral analysis:</i>		
Parameter (Unit)	Value	
Spectral type	F6 IV–V	
T_{eff} (K)	6400 ± 100	
$\log g_*$	3.9 ± 0.1	
[Fe/H]	-0.02 ± 0.05	
$v \sin i_*$ (km s ⁻¹)	13.8 ± 0.7	
v_{mic} (km s ⁻¹)	1.6 (assumed)	
v_{mac} (km s ⁻¹)	6.5 (assumed)	
<i>Parameters from photometric and RV analysis:</i>		
Parameter (Unit)	DT Value (adopted):	
P (d)	5.367753 ± 0.000004	
T_c (BJD _{TDB})	2457799.1256 ± 0.0007	
T_{14} (d)	0.186 ± 0.002	
$T_{12} = T_{34}$ (d)	0.017 ± 0.002	
R_p^2/R_*^2	0.0062 ± 0.0002	
b	0.45 ± 0.09	
i (°)	87.1 ± 0.7	
a (AU)	0.0663 ± 0.0008	
M_* (M_\odot)	1.35 ± 0.05	
R_* (R_\odot)	1.6 ± 0.1	
$\log g_*$ (cgs)	4.17 ± 0.04	
ρ_* (ρ_\odot)	0.34 ± 0.05	
T_{eff} (K)	6400 ± 100	
[Fe/H]	-0.02 ± 0.05	
K (km s ⁻¹)	0.099 ± 0.009	
M_p (M_{Jup})	1.0 ± 0.1	
R_p (R_{Jup})	1.15 ± 0.09	
$\log g_p$ (cgs)	3.2 ± 0.1	
T_{eq1} (K)	1500 ± 50	
<i>Parameters from RM and DT analyses:</i>		
Parameter (Unit)	DT Value (adopted):	RM Value:
γ (km s ⁻¹)	0.82 ± 0.01	0.823 ± 0.009
λ (°)	21 ± 6	23 ± 12
v_{FWHM} (km s ⁻¹)	10 ± 1	–
$v \sin i_*$ (km s ⁻¹)	13.3 ± 0.6	14.1 ± 0.7

Table 4. Parameters for WASP-190 from BAGEMASS:

Parameter (Unit)	Value
Age (Gyr)	2.8 ± 0.4
M_* (M_\odot)	1.30 ± 0.05
$[\text{Fe}/\text{H}]_{\text{init}}$	0.03 ± 0.04

calculated at each step using the Enoch–Torres relation (Enoch et al. 2010; Torres et al. 2010). The photometric data are displayed in Fig. 1 along with the best-fit model and residuals of the fit.

The RV analysis then enables measurement of the barycentric system velocity γ and the stellar reflex velocity semi-amplitude K_1 . We expect that most hot Jupiters will settle into a circular orbit on a shorter timescale than their lifetimes (Pont et al. 2011), but with an orbital period of ~ 5 days WASP-190b is entering the regime where eccentricity may remain. However, we do not have sufficient orbital RVs to constrain the eccentricity and so assume a circular orbit. The CORALIE data have larger error bars than the HARPS data, and the errors are underestimated since the CCFs are non-Gaussian. We do not include the CORALIE measurements in the model adopted here, though including them changes the planetary mass by much less than the error bar.

Both the RM analysis and the tomographic analysis allow the measurement of $v \sin i_*$ and λ , while providing an additional constraint on the values of γ and b . The tomographic analysis also requires that one fits the intrinsic line width of the perturbation to the CCF, v_{FWHM} , whose shape is assumed to be Gaussian. For each analysis we adopt the spectral $v \sin i_*$ as a prior.

We show all RV measurements used in this work, along with the best fitting RV and RM models in Fig. 3. We also display the tomographic data (the time series of CCFs with the average of the out-of-transit CCFs subtracted from all CCFs) in Fig. 4, along with the best-fit planet model and residuals. The best fit parameters are listed in Table 3. We adopt the solution to the tomographic analysis (see Section 6) and, to avoid duplicating parameters derived from the same data (which are consistent in any case), the only parameters for which we list values from both analyses are γ , $v \sin i_*$ and λ .

5. RESULTS FOR THE STAR

We find WASP-190 to be an inflated star, with $R_* = 1.6 \pm 0.1 R_\odot$ and $\rho_* = 0.34 \pm 0.05 \rho_\odot$. This implies that the star is beginning to evolve away from the main sequence, which would be consistent with the spectral type of F6 IV–V.

Using the InfraRed Flux Method (Blackwell & Shallics 1977) we measure the temperature of WASP-190 to

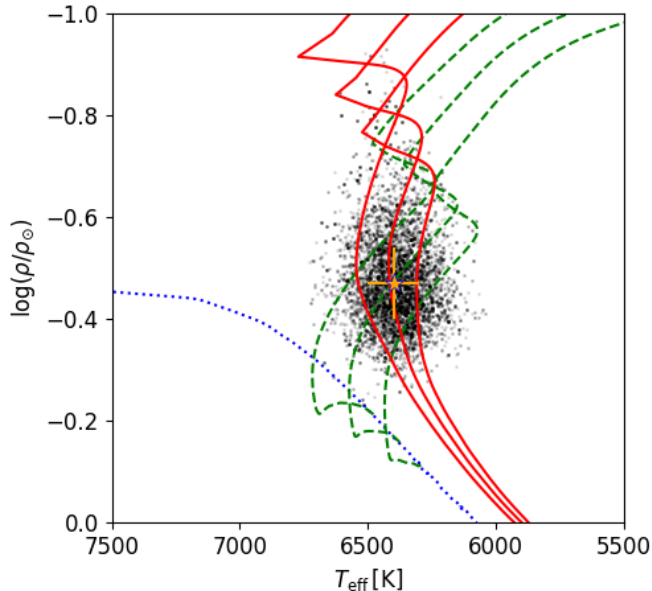


Figure 2. The best fitting evolutionary tracks and isochrones of WASP-190 obtained using BAGEMASS. Black points: individual realisations of the MCMC. Dotted blue line: Zero-Age Main Sequence (ZAMS) at best-fit $[\text{Fe}/\text{H}]$. Green dashed lines: evolutionary track for the best-fit $[\text{Fe}/\text{H}]$ and mass, plus 1σ bounds. Red lines: isochrone for the best-fit $[\text{Fe}/\text{H}]$ and age, plus 1σ bounds. Orange star: measured values of T_{eff} and ρ_* for WASP-190 obtained in the spectral and photometric analyses respectively.

be $T_{\text{eff}} = 6560 \pm 140$ K and the angular diameter θ to be 0.029 ± 0.001 mas. The *Gaia* DR2 (Gaia Collaboration et al. 2016, 2018) lists the parallax of WASP-190 as 1.82 ± 0.03 mas. Using these values and accounting for the correction to *Gaia* DR2 parallax values suggested by Stassun & Torres (2018), we obtain a stellar radius of $1.65 \pm 0.08 R_{\odot}$, which is consistent with our result from the MCMC analysis.

We investigate the age of WASP-190 using the open source software BAGEMASS¹ (Maxted et al. 2015). BAGEMASS allows the user to fit T_{eff} and M_* using stellar evolutionary models calculated for different He abundances and mixing lengths (GARSTEC; Weiss & Schlattl 2008). As inputs we use the values of T_{eff} and $[\text{Fe}/\text{H}]$ derived from the spectral analysis in Section 3, and also use the value of ρ_* obtained in the combined analysis (Section 4) as a constraint.

Assuming solar values for the He abundance and mixing length gave the best-fit solution. We display the corresponding isochrones and evolutionary tracks in Fig. 2. We find the current age of WASP-190 to be 2.8 ± 0.4 Gyr,

¹ <http://sourceforge.net/projects/bagemass>

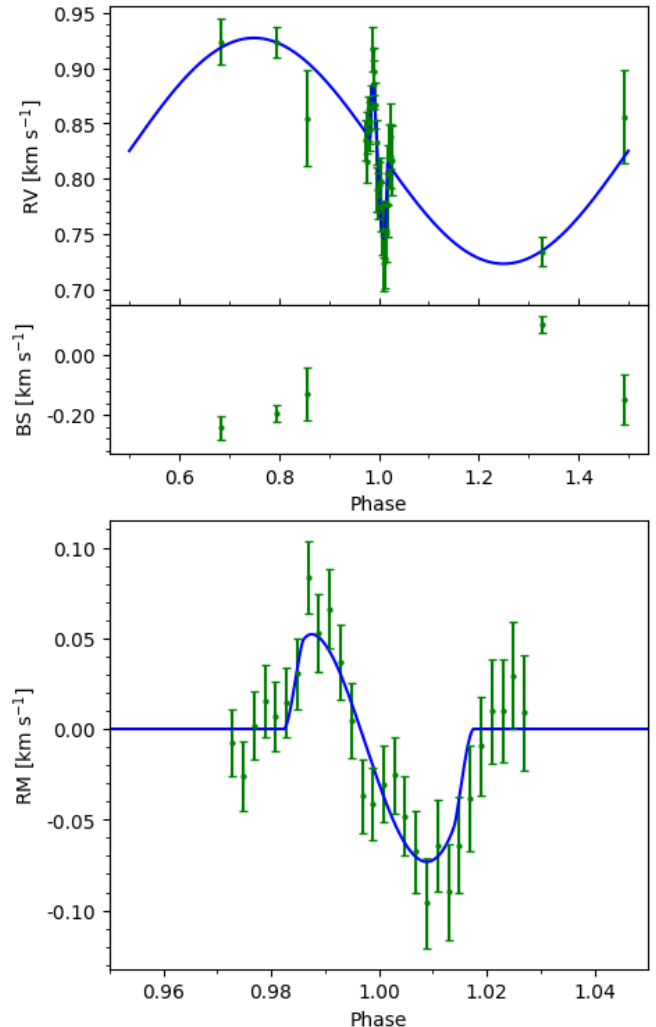


Figure 3. Top: The HARPS RV measurements used in the analysis of WASP-190b. The blue line shows the best-fit Keplerian RV curve and the fit to the RM effect. Centre: the bisectors for the out-of-transit RVs plotted against phase, which show no correlation with the RV measurements. Bottom: The region around transit on a larger scale.

implying that the star is beginning to evolve off the main sequence. This is consistent with our finding that the star is inflated. For comparison, the time taken to exhaust all hydrogen in the core is 3.8 ± 0.5 Gyr.

6. RESULTS FOR THE PLANET

We find a best fit K_1 of 0.099 ± 0.009 km s⁻¹, giving a planet mass of $M_p = 1.0 \pm 0.1 M_{\text{Jup}}$. The fitted planetary radius is $1.15 \pm 0.09 R_{\text{Jup}}$.

The in-transit RVs, showing the RM effect, are displayed in the lower panel of Fig. 3. The equivalent tomogram of the same data is shown in Fig. 4. Both are consistent with a planet in a prograde orbit. The pro-

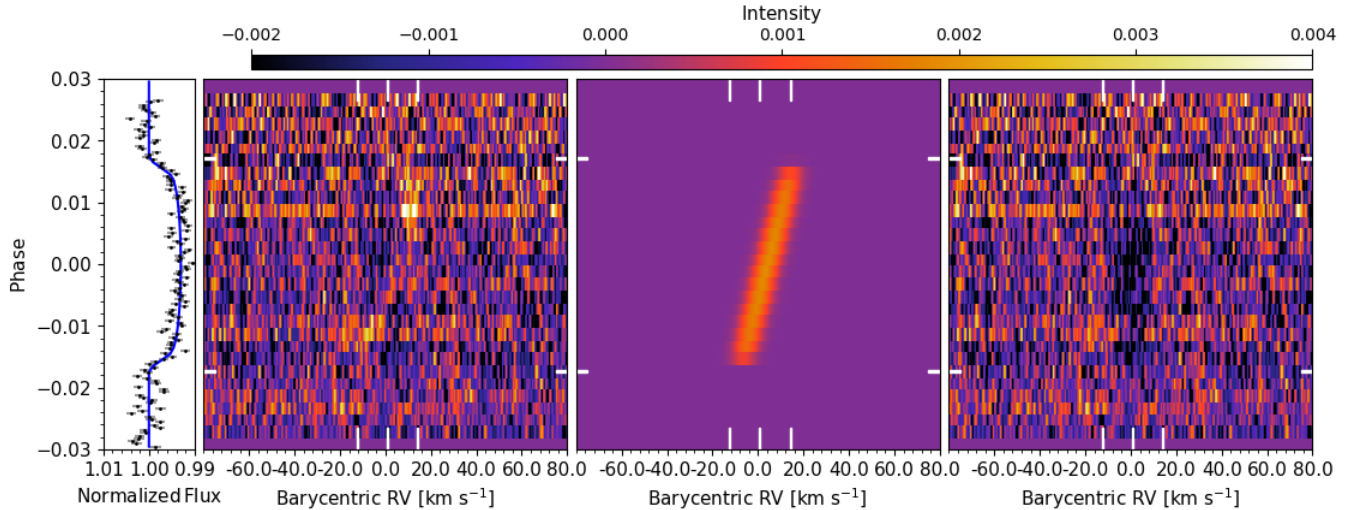


Figure 4. Centre-left: The Doppler tomogram comprised of the time series of residual HARPS CCFs calculated by subtracting the average of the out-of-transit CCFs from all CCFs. Left: the SPECULOOS-Europa lightcurve taken simultaneously with the HARPS observation. Centre-right: The best-fit planet model. Right: the residuals remaining after subtracting the best-fit planet model from the centre-left tomogram. In the three tomographic panels, the start and end times of the transit are marked with horizontal white dashes, while the vertical dashes mark respectively the positions of $\gamma - v \sin i_{\star}$, γ and $\gamma + v \sin i_{\star}$. We interpret the tomogram as showing a very faint, prograde planet signal which in places is completely masked by background noise.

jected spin-orbit angle, λ , is measured as $23 \pm 12^{\circ}$ in the RM analysis and as $21 \pm 6^{\circ}$ in the tomographic analysis. The planet trace is faint and hard to see, which we attribute to the star being relatively faint for tomographic analysis, at $V = 11.7$, and the transit dip being relatively shallow for a hot Jupiter, at 0.6%. The latter results from the star being relatively large at $1.6 R_{\odot}$ when compared to the planet, which has only a mildly inflated radius of $1.15 R_{\text{Jup}}$.

7. DISCUSSION AND CONCLUSIONS

We have shown that WASP-190b is a typical hot Jupiter with a mass of $1.0 \pm 0.1 M_{\text{Jup}}$ and a mildly inflated radius of $1.15 \pm 0.09 R_{\text{Jup}}$. It is in a 5.4-day orbit that is marginally misaligned with respect to the stellar rotation, with $\lambda = 21 \pm 6^{\circ}$.

The measured values of $v \sin i_{\star}$ and λ are consistent between the spectral analysis, the tomographic analysis and the RM analysis. The tomographic analysis produced similar fits, giving a $v \sin i_{\star}$ value consistent with the spectroscopic value, regardless of whether we adopted the spectroscopic $v \sin i_{\star}$ as a prior. In contrast, the RM analysis was less constrained without a prior, and the fit tended to favour values that were too large. This often occurs for systems with a low impact parameter b , since it is difficult to differentiate the effects of $v \sin i_{\star}$ and λ on the shape of the RM curve when it is symmetrical (e.g. Albrecht et al. 2011). Since, in WASP-190, the impact parameter has a mid-level value

of $b = 0.45$, this tendency should be reduced, but it may be that the low signal-to-noise of the data is leading the fit to be less constrained than usual. Overall, we found that the parameters were better constrained in the tomographic analysis than in the RM analysis, and so we adopt that fit.

While there is a well-established trend between the irradiation of a hot Jupiter and the inflation of its radius (e.g. Enoch et al. 2012), hot Jupiters also display a wide range of radii (e.g. Burrows et al. 2007). Sestovic et al. (2018) investigates the relationship between planet radius, mass and irradiation, finding that a more massive planet is usually less inflated than a low-mass planet of the same temperature, due to the planet’s gravity counteracting the inflation. In Fig. 5 we show planetary radius as a function of equilibrium temperature, and use planetary mass as a third dimension, for all planets with $0.6 M_{\text{Jup}} < M_{\text{p}} < 4.0 M_{\text{Jup}}$ as listed in the TEPcat database (Southworth 2011). The figure indicates that planets of a given mass can have a wide range of radii, and shows that planets of $\sim 1 M_{\text{Jup}}$ like WASP-190b are not necessarily inflated. Possible causes of the disparity include different evolutionary histories, leading to different amounts of irradiation over time (e.g. Hartman et al. 2016), the possibility of internal heating mechanisms (e.g. Kurokawa & Inutsuka 2015; Ginzburg & Sari 2015; Thorngren & Fortney 2018; Ryu et al. 2018) and differences in the mass and metallicity of the planets’ cores (e.g. Enoch et al. 2012).

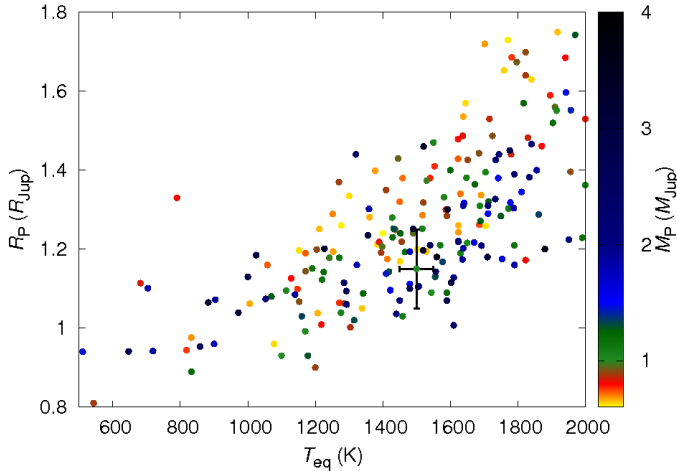


Figure 5. R_p vs. T_{eq} , colour coded by mass, of all known planets with $0.6 M_{\text{Jup}} < M_p < 4.0 M_{\text{Jup}}$. WASP-190b is displayed including the error bars on the measured radius and temperature.

With $\lambda = 21 \pm 6^\circ$, WASP-190b is marginally misaligned. This is consistent with the known trend in hot-star systems, whereby planets around stars beyond the Kraft break have a wider range of obliquities, with most being in misaligned orbits (e.g. Winn et al. 2010; Dai & Winn 2017). The true orbit may be more strongly misaligned, however, since the value of $|\lambda|$ for non-polar misaligned orbits represents a lower limit for the true obliquity $|\psi|$. To measure ψ it would be necessary to independently measure the stellar equatorial rotational

velocity v or stellar inclination i_\star (for example, by looking for differential rotation effects as described by Cegla et al. 2016).

WASP-South is hosted by the South African Astronomical Observatory and we are grateful for their ongoing support and assistance. Funding for WASP comes from consortium universities and from the UK’s Science and Technology Facilities Council. The research leading to these results has received funding from the European Research Council (ERC) under the FP/2007-2013 ERC grant agreement no. 336480, and under the H2020 ERC grant agreement no. 679030; and from an Actions de Recherche Concertée (ARC) grant, financed by the Wallonia-Brussels Federation. The Euler Swiss telescope is supported by the Swiss National Science Foundation (SNF). TRAPPIST-South is funded by the Belgian Fund for Scientific Research (Fond National de la Recherche Scientifique, FNRS) under the grant FRFC 2.5.594.09.F, with the participation of the SNF. M. Gillon and E. Jehin are F.R.S.-FNRS Senior Research Associates. We acknowledge use of the ESO 3.6-m/HARPS spectrograph under programs 0100.C-0847(A), PI C. Hellier, and 0102.C-0414, PI L. Nielsen.

Facilities: SuperWASP, ESO:3.6m(HARPS), Euler1.2m(CORALIE), WASP-South, TRAPPIST, SPECULOOS Southern Observatory (SSO)

REFERENCES

- Albrecht, S., Winn, J. N., Johnson, J. A., et al. 2011, *ApJ*, 738, 50, doi: [10.1088/0004-637X/738/1/50](https://doi.org/10.1088/0004-637X/738/1/50)
- Anderson, D. R., Temple, L. Y., Nielsen, L. D., et al. 2018, ArXiv e-prints. <https://arxiv.org/abs/1809.04897>
- Baranne, A., Queloz, D., Mayor, M., et al. 1996, *A&AS*, 119, 373
- Blackwell, D. E., & Shallis, M. J. 1977, *MNRAS*, 180, 177, doi: [10.1093/mnras/180.2.177](https://doi.org/10.1093/mnras/180.2.177)
- Boué, G., Montalto, M., Boisse, I., Oshagh, M., & Santos, N. C. 2013, *A&A*, 550, A53, doi: [10.1051/0004-6361/201220146](https://doi.org/10.1051/0004-6361/201220146)
- Brown, D. J. A., Triaud, A. H. M. J., Doyle, A. P., et al. 2017, *MNRAS*, 464, 810, doi: [10.1093/mnras/stw2316](https://doi.org/10.1093/mnras/stw2316)
- Bruntt, H., Bedding, T. R., Quirion, P.-O., et al. 2010, *MNRAS*, 405, 1907, doi: [10.1111/j.1365-2966.2010.16575.x](https://doi.org/10.1111/j.1365-2966.2010.16575.x)
- Burdanov, A., Delrez, L., Gillon, M., & Jehin, E. 2018, *SPECULOOS Exoplanet Search and Its Prototype on TRAPPIST*, ed. H. J. Deeg & J. A. Belmonte (Cham: Springer International Publishing), 1–17. https://doi.org/10.1007/978-3-319-30648-3_130-1
- Burrows, A., Hubeny, I., Budaj, J., & Hubbard, W. B. 2007, *ApJ*, 661, 502, doi: [10.1086/514326](https://doi.org/10.1086/514326)
- Cegla, H. M., Lovis, C., Bourrier, V., et al. 2016, *A&A*, 588, A127, doi: [10.1051/0004-6361/201527794](https://doi.org/10.1051/0004-6361/201527794)
- Claret, A. 2000, *A&A*, 363, 1081
- . 2004, *A&A*, 428, 1001, doi: [10.1051/0004-6361:20041673](https://doi.org/10.1051/0004-6361:20041673)
- Collier Cameron, A., Bruce, V. A., Miller, G. R. M., Triaud, A. H. M. J., & Queloz, D. 2010a, *MNRAS*, 403, 151, doi: [10.1111/j.1365-2966.2009.16131.x](https://doi.org/10.1111/j.1365-2966.2009.16131.x)
- Collier Cameron, A., Wilson, D. M., West, R. G., et al. 2007, *MNRAS*, 380, 1230, doi: [10.1111/j.1365-2966.2007.12195.x](https://doi.org/10.1111/j.1365-2966.2007.12195.x)

- Collier Cameron, A., Guenther, E., Smalley, B., et al. 2010b, *MNRAS*, 407, 507, doi: [10.1111/j.1365-2966.2010.16922.x](https://doi.org/10.1111/j.1365-2966.2010.16922.x)
- Dai, F., & Winn, J. N. 2017, *AJ*, 153, 205, doi: [10.3847/1538-3881/aa65d1](https://doi.org/10.3847/1538-3881/aa65d1)
- Delrez, L., Gillon, M., Queloz, D., et al. 2018, in *Society of Photo-Optical Instrumentation Engineers (SPIE) Conference Series*, Vol. 10700, *Society of Photo-Optical Instrumentation Engineers (SPIE) Conference Series*, 107001I
- Doyle, A. P., Davies, G. R., Smalley, B., Chaplin, W. J., & Elsworth, Y. 2014, *MNRAS*, 444, 3592, doi: [10.1093/mnras/stu1692](https://doi.org/10.1093/mnras/stu1692)
- Enoch, B., Collier Cameron, A., & Horne, K. 2012, *A&A*, 540, A99, doi: [10.1051/0004-6361/201117317](https://doi.org/10.1051/0004-6361/201117317)
- Enoch, B., Collier Cameron, A., Parley, N. R., & Hebb, L. 2010, *A&A*, 516, A33, doi: [10.1051/0004-6361/201014326](https://doi.org/10.1051/0004-6361/201014326)
- Gaia Collaboration, Prusti, T., de Bruijne, J. H. J., et al. 2016, *A&A*, 595, A1, doi: [10.1051/0004-6361/201629272](https://doi.org/10.1051/0004-6361/201629272)
- Gaia Collaboration, Brown, A. G. A., Vallenari, A., et al. 2018, *A&A*, 616, A1, doi: [10.1051/0004-6361/201833051](https://doi.org/10.1051/0004-6361/201833051)
- Gillon, M. 2018, *Nature Astronomy*, 2, 344, doi: [10.1038/s41550-018-0443-y](https://doi.org/10.1038/s41550-018-0443-y)
- Ginzburg, S., & Sari, R. 2015, *ApJ*, 803, 111, doi: [10.1088/0004-637X/803/2/111](https://doi.org/10.1088/0004-637X/803/2/111)
- Gray, R. O., & Corbally, C. J. 2014, *AJ*, 147, 80, doi: [10.1088/0004-6256/147/4/80](https://doi.org/10.1088/0004-6256/147/4/80)
- Hartman, J. D., Bakos, G. Á., Bhatti, W., et al. 2016, *AJ*, 152, 182, doi: [10.3847/0004-6256/152/6/182](https://doi.org/10.3847/0004-6256/152/6/182)
- Hellier, C., Anderson, D. R., Collier Cameron, A., et al. 2011, in *European Physical Journal Web of Conferences*, Vol. 11, *European Physical Journal Web of Conferences*, 01004
- Hirano, T., Suto, Y., Winn, J. N., et al. 2011, *ApJ*, 742, 69, doi: [10.1088/0004-637X/742/2/69](https://doi.org/10.1088/0004-637X/742/2/69)
- Jehin, E., Gillon, M., Queloz, D., et al. 2011, *The Messenger*, 145, 2
- Kurokawa, H., & Inutsuka, S.-i. 2015, *ApJ*, 815, 78, doi: [10.1088/0004-637X/815/1/78](https://doi.org/10.1088/0004-637X/815/1/78)
- Lund, M. B., Rodriguez, J. E., Zhou, G., et al. 2017, *AJ*, 154, 194, doi: [10.3847/1538-3881/aa8f95](https://doi.org/10.3847/1538-3881/aa8f95)
- Maxted, P. F. L., Serenelli, A. M., & Southworth, J. 2015, *A&A*, 575, A36, doi: [10.1051/0004-6361/201425331](https://doi.org/10.1051/0004-6361/201425331)
- Maxted, P. F. L., Anderson, D. R., Collier Cameron, A., et al. 2011, *PASP*, 123, 547, doi: [10.1086/660007](https://doi.org/10.1086/660007)
- Pepe, F., Mayor, M., Rupprecht, G., et al. 2002, *The Messenger*, 110, 9
- Pollacco, D., Skillen, I., Collier Cameron, A., et al. 2008, *MNRAS*, 385, 1576, doi: [10.1111/j.1365-2966.2008.12939.x](https://doi.org/10.1111/j.1365-2966.2008.12939.x)
- Pont, F., Husnoo, N., Mazeh, T., & Fabrycky, D. 2011, *MNRAS*, 414, 1278, doi: [10.1111/j.1365-2966.2011.18462.x](https://doi.org/10.1111/j.1365-2966.2011.18462.x)
- Queloz, D., Eggenberger, A., Mayor, M., et al. 2000, *A&A*, 359, L13
- Queloz, D., Mayor, M., Udry, S., et al. 2001, *The Messenger*, 105, 1
- Ricker, G. R., Winn, J. N., Vanderspek, R., et al. 2015, *Journal of Astronomical Telescopes, Instruments, and Systems*, 1, 014003, doi: [10.1117/1.JATIS.1.1.014003](https://doi.org/10.1117/1.JATIS.1.1.014003)
- Ryu, T., Zingale, M., & Perna, R. 2018, *MNRAS*, 481, 5517, doi: [10.1093/mnras/sty2638](https://doi.org/10.1093/mnras/sty2638)
- Sestovic, M., Demory, B.-O., & Queloz, D. 2018, *A&A*, 616, A76, doi: [10.1051/0004-6361/201731454](https://doi.org/10.1051/0004-6361/201731454)
- Southworth, J. 2011, *MNRAS*, 417, 2166, doi: [10.1111/j.1365-2966.2011.19399.x](https://doi.org/10.1111/j.1365-2966.2011.19399.x)
- Stassun, K. G., & Torres, G. 2018, *ApJ*, 862, 61, doi: [10.3847/1538-4357/aacafc](https://doi.org/10.3847/1538-4357/aacafc)
- Stassun, K. G., Oelkers, R. J., Pepper, J., et al. 2018, *AJ*, 156, 102, doi: [10.3847/1538-3881/aad050](https://doi.org/10.3847/1538-3881/aad050)
- Talens, G. J. J., Albrecht, S., Spronck, J. F. P., et al. 2017, *A&A*, 606, A73, doi: [10.1051/0004-6361/201731282](https://doi.org/10.1051/0004-6361/201731282)
- Temple, L. Y., Hellier, C., Albrow, M. D., et al. 2017, *MNRAS*, 471, 2743, doi: [10.1093/mnras/stx1729](https://doi.org/10.1093/mnras/stx1729)
- Temple, L. Y., Hellier, C., Almleaky, Y., et al. 2018, *MNRAS*, 480, 5307, doi: [10.1093/mnras/sty2197](https://doi.org/10.1093/mnras/sty2197)
- Thorngren, D. P., & Fortney, J. J. 2018, *AJ*, 155, 214, doi: [10.3847/1538-3881/aaba13](https://doi.org/10.3847/1538-3881/aaba13)
- Torres, G., Andersen, J., & Giménez, A. 2010, *A&A Rv*, 18, 67, doi: [10.1007/s00159-009-0025-1](https://doi.org/10.1007/s00159-009-0025-1)
- Triaud, A. H. M. J. 2017, *The Rossiter–McLaughlin Effect in Exoplanet Research*, ed. H. J. Deeg & J. A. Belmonte (Cham: Springer International Publishing), 1–27. https://doi.org/10.1007/978-3-319-30648-3_2-1
- Weiss, A., & Schlattl, H. 2008, *Ap&SS*, 316, 99, doi: [10.1007/s10509-007-9606-5](https://doi.org/10.1007/s10509-007-9606-5)
- Winn, J. N., Fabrycky, D., Albrecht, S., & Johnson, J. A. 2010, *ApJL*, 718, L145, doi: [10.1088/2041-8205/718/2/L145](https://doi.org/10.1088/2041-8205/718/2/L145)
- Zhou, G., Bakos, G. Á., Hartman, J. D., et al. 2017, *AJ*, 153, 211, doi: [10.3847/1538-3881/aa674a](https://doi.org/10.3847/1538-3881/aa674a)